Int. J. Microgravity Sci. Appl., **36** (3) (2019) 360306
DOI: 10.15011//jasma.36.360306

IIII Original Paper IIII

Improvement in Phase Analysis using Spatio-Temporal Images for Soret Coefficient Measurements

Isamu ORIKASA [1], Takuma OSADA [1], Momoko TOMARU [1], Shinsuke SUZUKI [2,3,4] and Yuko INATOMI [5,6]

Abstract

The *Soret-Facet Mission* was conducted in microgravity to measure the Soret coefficient S_T using a two-wavelength Mach-Zehnder Interferometer (2-MZI). Interferometer analysis generally uses procedures like fringe tracing (thinning method) that impede processing speed and accuracy. In the present study, an automated phase analysis using spatio-temporal images was developed based on the simple conversion of intensity $I(t)$ into phase $\phi(t)$. This automatically analyzes steps, starting with obtaining the spatio-temporal images of moving interference fringes to calculating phase change $\Delta\phi(t)$. It dramatically improved processing speed and larger analyzing areas compared to the thinning method. Applying filters and a threshold to the fringes using suitable conditions—which the method determined automatically and quickly—was confirmed to be efficient for the correct unwrapping of phase.

Keyword(s): Interferometer, Phase analysis, Spatio-temporal images, Soret effect, *Soret-Facet Mission*.

Received 30 December 2018, Accepted 23 April 2019, Published 31 July 2019

1. Introduction

The temperature gradient induces the molecule diffusion in mixtures, which is called the Soret effect. It is an important diffusion phenomenon and it plays an important role in solute redistribution during crystal growth [1]. The Soret effect is quantified by the Soret coefficient (S_T). To understand the Soret effect, the accurate measurements of Soret coefficients are critical. Then, in the *Soret-Facet Mission* [2], Soret coefficients in binary mixtures were measured using a two-wavelength Mach-Zehnder Interferometer (2-MZI) in the Kibo module in the ISS, where the disturbance caused by the convection could be suppressed.

An interferometer with laser beams of two different wavelengths can measure very fine temperature and concentration changes (ΔT and ΔC, respectively), caused in a transparent sample solution, without physical contact. They are measured as phase change $\Delta\phi$ of the fringes (Eq. 1) [2].

$$\Delta\phi = \frac{2\pi d}{\lambda}(n_{\mathrm{T}}\Delta T + n_{\mathrm{C}}\Delta C) \tag{1}$$

Here, d is the thickness of sample and λ is the wavelength of the laser beam. The symbols n_{T} and n_{C} are the temperature and concentration coefficients of refractive indices, respectively. Therefore, the accurate measurements of the phase change $\Delta\phi$ are critical for the accurate measurements of the Soret coefficients.

The fringe tracing method that uses thinning fringes [3,4] (in this paper, this method is called "thinning method") has been applied for the analysis of the experimental results obtained in *Soret-Facet* Mission [5,6]. In this method, the values of $\Delta\phi$ can be measured by simply counting the number of fringes passing over an arbitrary position, using which the phase could be calculated

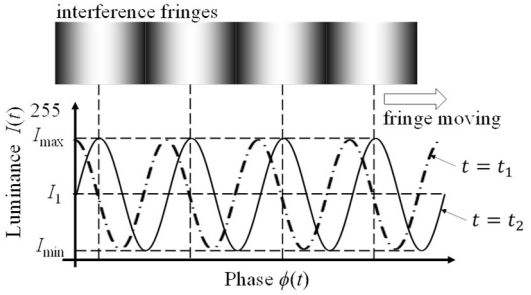

Fig. 1 Schematic diagram of relationship between intensity $I(t)$ and phase $\phi(t)$ of interference fringes at times of t_1 and t_2.

1 Faculty of Science and Engineering, Waseda University, Tokyo 169-8555, Japan.
2 Department of Applied Mechanics and Aerospace Engineering, Waseda University, Tokyo 169-8555, Japan.
3 Kagami Memorial Research Institute of Materials Science and Technology, Waseda University, Tokyo 169-8555, Japan.
4 Department of Materials Science, Waseda University, Tokyo 169-8555, Japan.
5 Institute of Space and Astronautical Science, Japan Aerospace Exploration Agency, 3-1-1 Yoshinodai, Chuo-ku, Sagamihara, Kanagawa 252-5210, Japan.
6 School of Physical Sciences, SOKENDAI (The Graduate University for Advanced Studies), 3-1-1 Yoshinodai, Chuo-ku, Sagamihara, Kanagawa 252-5210, Japan.
(E-mail: i.orikasa@fuji.waseda.jp)

independently and easily for each pixel. This leads to avoidance of interference between pixels. However, the thinning method requires manual procedures [4] during calculating the number of passing fringes, which act as obstacles for increasing processing speed and improvement of accuracy due to increase in number of measurement points. Furthermore, it is not possible to analyze the thinned interference fringes broken and combined. Therefore, it is difficult to analyze the interference fringes in whole areas of observation using the thinning method.

In the field of research dealing with shape and deformation measurements of specimens, fringe analysis methods were developed using phase analysis [7]. In phase analysis, fringes are considered as a sine curve of intensity $I(t)$ at a time t as follows (the schematic diagram is shown in **Fig. 1**):

$$I(t) = I_0 \sin\phi(t) + I_1 \tag{2}$$

Here, $\phi(t)$ is the phase at a time t, I_0 $(= (I_{\max} - I_{\min})/2)$ is the amplitude, and I_1 $(= (I_{\max} + I_{\min})/2)$ is the center value of the amplitude, where $I_{\max}$ and $I_{\min}$ are the maximum and minimum values of $I(t)$, respectively. The values of $I_{\max}$ and $I_{\min}$ correspond to the intensity of the center of light and dark fringes, respectively. The common methods for measuring phase $\phi(t)$ are the phase shifting technique [8,9] and the Fourier transform technique [10]. In the research field of thermodiffusion, Mialdun and his co-workers developed these techniques [11–13]. However, the phase shifting technique needs phase shifters [14]. In the Fourier transform technique, the definition of the distance between interference fringes and resolution of images are critical, and depend on the researchers. In the experiment, the influence of the air disturbance around sample solutions should be excluded.

Therefore, we focused on simple phase analysis to obtain the following equation:

$$\phi(t) = \arcsin\left(\frac{2I(t) - I_{\max} - I_{\min}}{I_{\max} - I_{\min}}\right) \tag{3}$$

Eq. 3 was modified from Eq. 2. Using Eq. 3, the intensity $I(t)$ can be converted into the phase $\phi(t)$ simply by obtaining the values of $I_{\max}$ and $I_{\min}$. In spatio-temporal images of interference fringes, the values of $\phi(t)$ repeatedly become $-\pi/2$ and $\pi/2$ when the center of dark and light fringes pass over an arbitrary pixel, that is, when the values of $I(t)$ are maximum and minimum, respectively. Therefore, detecting the maximal and minimal values of $\phi(t)$ enables us to unwrap the values of $\phi(t)$ and calculate the phase change $\Delta\phi$.

The objective of this study is to improve a simple automated phase analysis method. This paper reports the effectiveness of the simple automated phase analysis algorithm by directly converting intensity $I(t)$ to phase $\phi(t)$, which is processed through filters and a threshold for the fringes (called "proposed method" in the following discussion), which was applied to the experimental results obtained in the *Soret-Facet Mission* [2]. In the reference paper [2], the Soret coefficient of salol - 2.58 wt. % tert-butyl alcohol was obtained by using the proposed method in this study. The remainder of this paper is organized as follows. The experimental and analysis procedures are discussed in Sec. 2. Sec. 3 describes the results of applying the proposed method before processing through filters and a threshold to the simulated fringes and the experimental fringes. The effectiveness of processing through filters and a threshold for the noise exclusion, and the universality of the proposed method are discussed in Sec. 4. The study is concluded in Sec. 5.

2. Experimental and Analysis Procedures for Obtaining the Phase Change $\Delta\phi$

2.1 Experimental Apparatus and Procedures

The experimental procedure is the same as that described in a reference paper of our group[5]. By using the following facility already set up in Japanese Experiment Module (JEM), "*Kibo*" of International Space Station (ISS), Soret effect experiments were performed. **Figure 2** shows the sample module set in a two-wavelength Mach-Zehnder Interferometer in the Solution Crystallization Observation Facilities (SCOF). The sample solution was salol - 1.15 wt. % tert-butyl alcohol in a sample cell made of quartz, called *Facet-Cell* [3]. The length of the cell in the height direction given the temperature gradient was 16 mm. The width of the cell was 4.8 mm. The length of the cell in the depth direction through which laser beams passed was 1 mm, that is, the value of d was 1 mm.

In this study, the data obtained in an experimental run (RUN #1-09) were analyzed as an example. The sample solution was heated up by Peltier devices set on both ends of the sample cell and held at 60 °C for 7 h to homogenize the temperature and concentration. Then, the temperature of one end was lowered to 30 °C and held at the temperature. In this paper, the time t corresponds to the holding time immediately after lowering temperature of the end. During holding and changing temperature, the interference fringes were observed and recorded by a CCD camera (480 × 640 pixels) for approximately 7 h. The size of the observation field was 2.4 × 3.2 mm^2. Two laser beams with wavelengths of 532 nm and 780 nm were irradiated alternately in

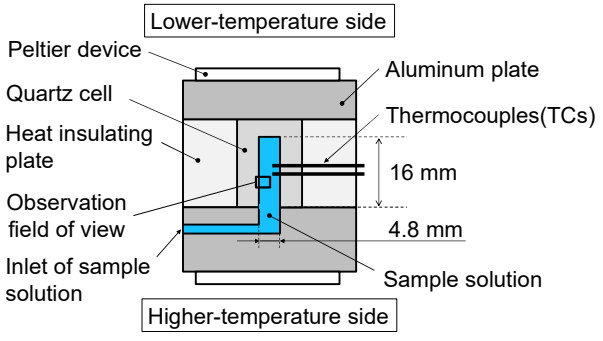

Fig. 2 Schematic diagrams of sample module set in a two-wavelength Mach-Zehnder Interferometer in the Solution Crystallization Observation Facilities (SCOF) modified from a reference[2]. The size of the inner cavity of the quartz cell was 16 × 4.8 × 1 mm^3, and that of observation field was 2.4 ×3.2 mm^2.

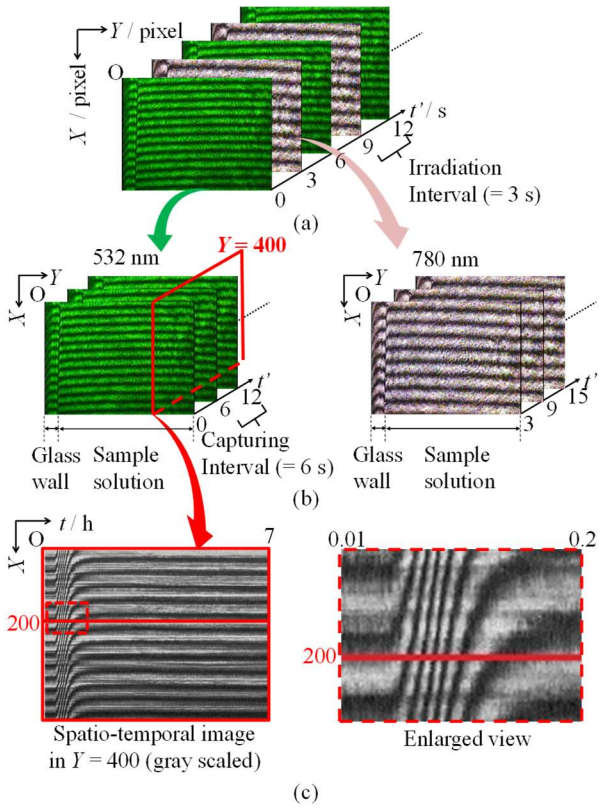

Fig. 3 Examples of interference fringes. (a) Moving images where two laser beams ($\lambda = 532$ and 780 nm) were irradiated alternately in 3 s intervals (the value of $t'(= t \cdot 3600\ \mathrm{s})$ corresponds to the holding time and the values of X and Y correspond to the pixels in the vertical and horizontal directions of the images, respectively), (b) captured images every 6 s, that is, 2 irradiation intervals, and (c) gray scaled spatio-temporal image in a line $Y = 400$ in wavelength 532 nm and the enlarged view (the value of t corresponds to the holding time).

3 s intervals. **Figure 3 (a)** shows the moving images for both the wavelengths. The value of $t'(= t \cdot 3600\ \mathrm{s})$ corresponds to the holding time and the values of X and Y correspond to the pixels in the vertical and horizontal directions of the images, respectively.

2.2 Analysis Procedures

By using the algorithm developed in this study, the phase change $\Delta\phi$ was calculated through simple conversion of intensity $I(t)$ into phase $\phi(t)$. The procedure for calculating the value of $\Delta\phi_{(X,Y)}$ at an arbitrary pixel (X, Y) consists of six steps as shown in **Fig. 4**. The green blocks with a double square **(Figs. 4 (a2), (e2), and (f2))** were skipped in the preliminary procedure, and done in the completed procedure explained in the discussion. Before executing this procedure, RGB still images (480×640 pixels) were captured every 6 s from the recorded moving images (**Fig. 3 (b)**) and converted into gray scaled ones.

1st step) Focusing on a spatio-temporal image in an arbitrary value of Y and obtaining intensity $I(t)_{(X,Y)}$ in an arbitrary value of X. **Figure 3 (c)** shows the example spatio-temporal image of the experiment in a line $Y = 400$.

2nd step) Detecting the maximum $I_{\max_{(X,Y)}}$ and minimum $I_{\min_{(X,Y)}}$ of $I(t)_{(X,Y)}$.

3rd step) Calculating phase $\phi(t)_{(X,Y)}$ by substituting the values of $I(t)_{(X,Y)}$, $I_{\max_{(X,Y)}}$, and $I_{\min_{(X,Y)}}$ into Eq. 3.

4th step) Detecting maximal and minimal values $\phi_{\mathrm{P}_{(X,Y)}}$ (called "peak values" in the following discussion) of $\phi(t)_{(X,Y)}$ using the *findpeaks* function in MATLAB®. Here, the k-th detected peak values and the time are defined as ϕ_{P_k} and t_k, respectively. When the peak values were maximal, the detected peak values were defined to begin with ϕ_{P_1}, and then followed by $k = 2, 3, \cdots, n$. When the peak values were minimal, the detected peak values were defined to begin with ϕ_{P_0}, and then followed by $k = 1, 2, \cdots, n-1$. The number of detected peak values was defined as n.

5th step) Unwrapping the phase into the values of $\phi'(t)_{(X,Y)}$ n times. For each k-th unwrapping, the unwrapped phase $\phi'_k(t)$ was inverted in a line $\phi'(t)_{(X,Y)} = \phi_{\mathrm{k}}$ (Eq. 4) symmetrically according to Eq. 5. In Eq. 5, the period of times from $t_0\ t_1$ was not defined because it was unnecessary for the phase of the period to be unwrapped.

$$\phi_{\mathrm{k}} = \frac{\pi}{2} + (k-1)\pi \quad \text{for } t \geq t_{\mathrm{k}}\ (k = 1, 2, \cdots, n),\ t \leq t_{\mathrm{k}}\ (k = 0) \tag{4}$$

$$\phi'_k(t) = 2\phi_{\mathrm{k}} - \phi'_{k-1}(t) \quad \text{for } t \geq t_{\mathrm{k}}\ (k = 1, 2, \cdots, n),\ t \leq t_{\mathrm{k}}\ (k = 0) \tag{5}$$

6th step) Obtaining the phase change $\Delta\phi_{(X,Y)} = \phi'(7\ \mathrm{h})_{(X,Y)} - \phi'(0\ \mathrm{h})_{(X,Y)}$.

The 1st–6th steps were repeated using other values of X and Y to calculate the spatial distribution of the values of $\Delta\phi_{(X,Y)}$.

3. Results of Applying the Proposed Method to the Simulated and the Experimental Fringes

First, the proposed method was applied to 100 sheets of the simulated moving interference fringe images (480×640 pixels). These images consisted of chirp signals in which the frequency increased with time. As shown in **Figs. 4 (c) to (f1)**, the intensity and phase were obtained in the 1st to 3rd steps, and three maximal and four minimal peak values were detected in the 4th step. The number of the detected peak values was coincident with that obtained from the spatio-temporal image in **Fig. 4 (b)**. The phase was then unwrapped seven times and the phase change was calculated as shown in **Fig. 4 (h)**. Furthermore, the spatial

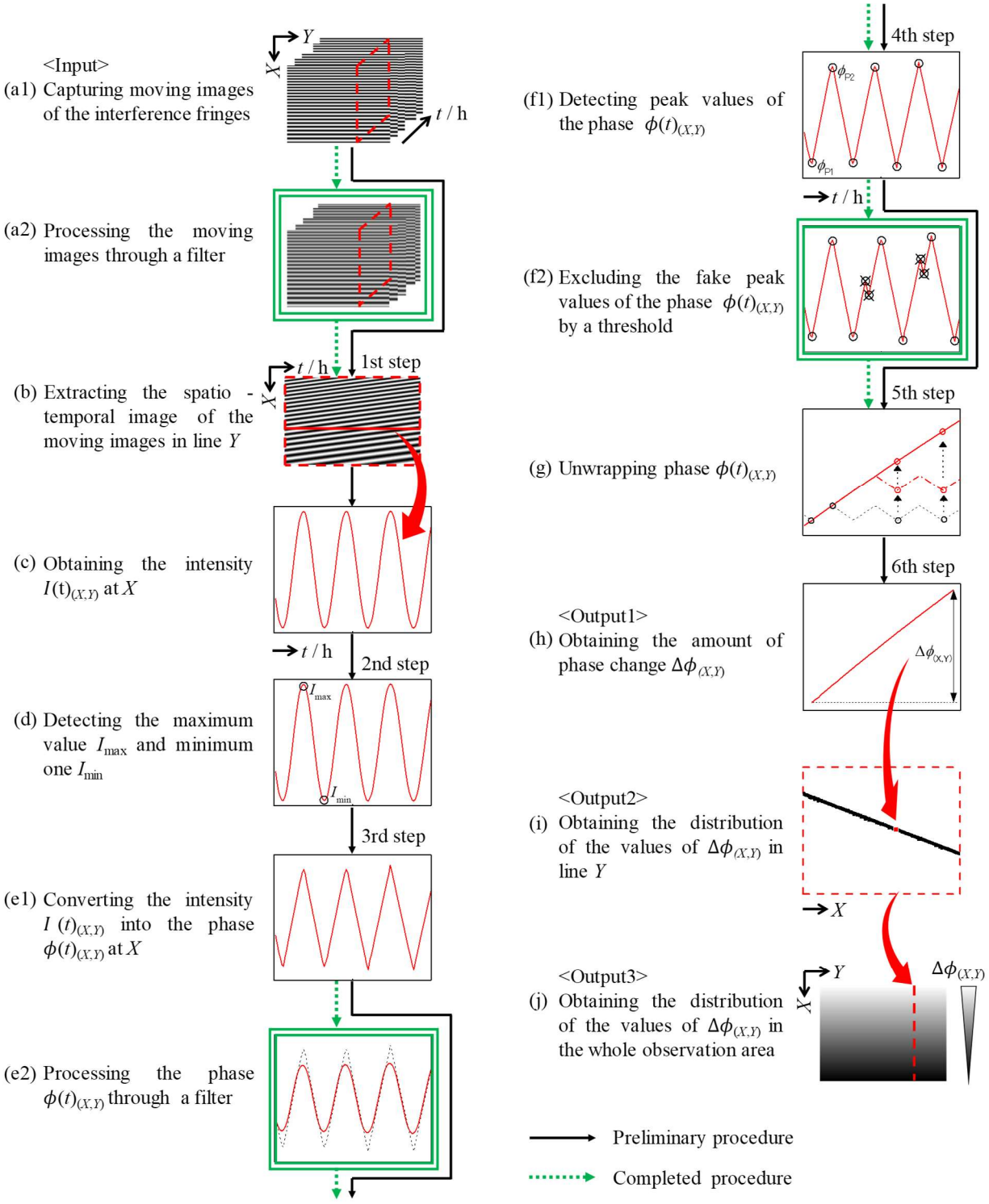

Fig. 4 Algorithm of the proposed method in this study for calculating the value of $\Delta\phi$. The green blocks with a double square (a2, e2, and f2) were skipped in the preliminary procedure, and done in the completed procedure explained in the discussion.

distribution of phase change in the whole observation area was obtained as shown in **Fig. 4 (j)**. Therefore, accurate operation of the algorithm was confirmed. In the experiment, interference fringes in wavelength 532 nm moved forward to the top side from 0 h to around 0.25 h and moved forward to the bottom side from approximately 0.25 h to the end as shown in **Fig. 3 (c)**. As an example, in X = 200 in the enlarged view of **Fig. 3 (c)**, approximately six dark and six bright fringes could be confirmed to have passed from approximately 0.03 h to 0.15 h. In the following discussion, the results of each step at the pixel (200,

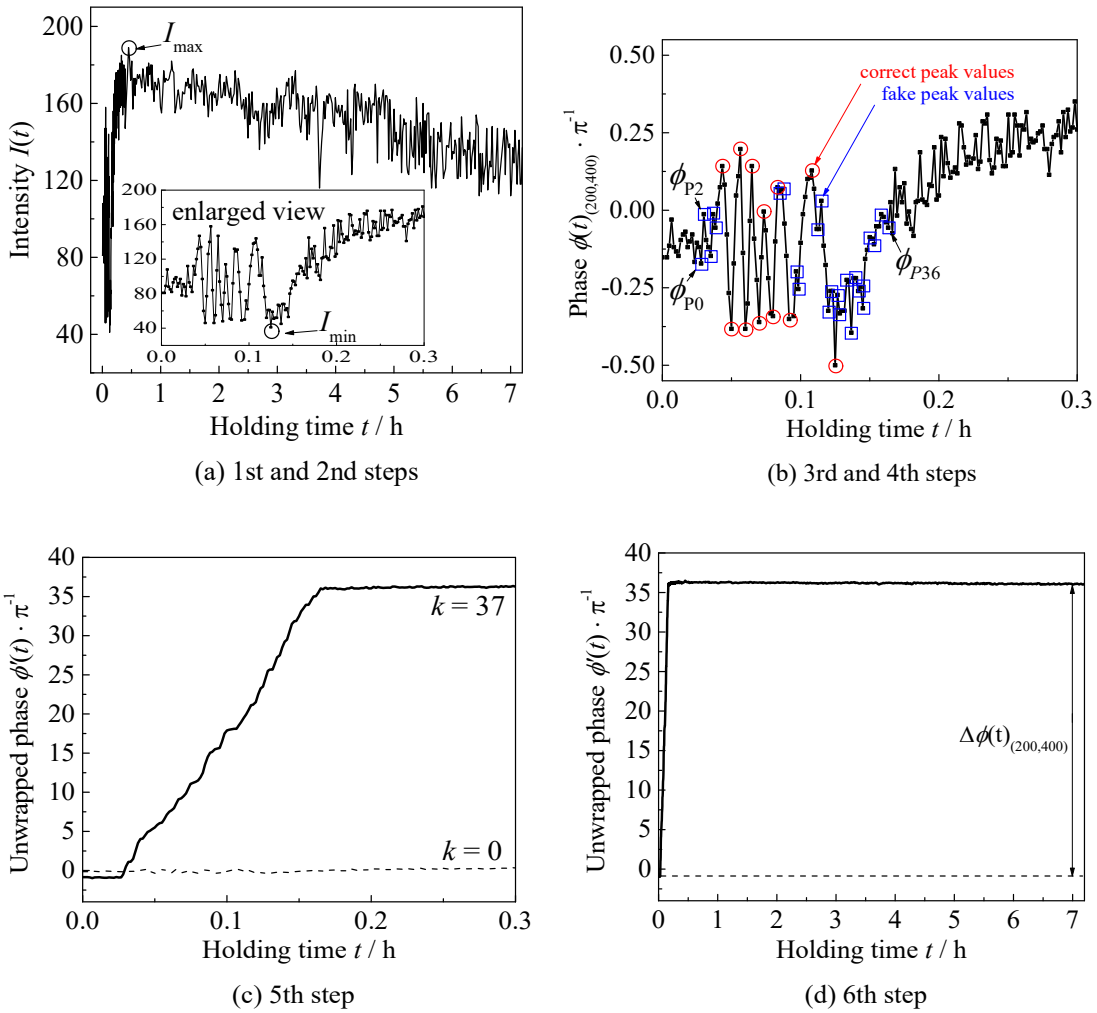

Fig. 5 Results from the 1st to the 5th steps of the proposed method at a pixel (200, 400) of wavelength 532 nm. (a) Intensity $I(t)_{(200,400)}$ obtained in the 1st step and the maximum $I_{\max(200,400)}$ and the minimum intensity $I_{\min(200,400)}$ obtained in the 2nd step: the solid black squares plot the results obtained every 6 s and the solid line shows the connected ones. (b) Phase $\phi(t)_{(200,400)}$ normalized by π rad converted in the 3rd step and detected peak values in the 4th step: blank red circles and blank blue squares plot correct and fake peak values, respectively, and the values of ϕ_{P_k} correspond to the *k*–th detected peak values. (c) Unwrapped phase $\phi'(t)_{(200,400)}$ obtained in the 5th step (dotted and solid line correspond to the original phase and unwrapped phase after 37 times unwrapping, respectively), and (d) whole view of the values of $\phi'(t)_{(200,400)}$ and the phase change $\Delta\phi(t)_{(200,400)} = \phi'(7\text{ h})_{(200,400)} - \phi'(0\text{ h})_{(200,400)}$.

400) in wavelength 532 nm have been mentioned.

In the 1st step, intensity $I(t)_{(200,400)}$ at pixel (200, 400) was obtained as shown in **Fig. 5 (a)**. The values of $I(t)_{(200,400)}$ changed largely from approximately 0.03 h. These intensity changes were caused by temperature change of sample solution. Peak values of these large intensity changes mean that interference fringes passed over the pixel. The maximal and minimal values correspond to bright and dark fringes, respectively. Therefore, in the enlarged view of **Fig. 5 (a)**, six maximal values and six minimal values from approximately 0.03 h to 0.13 h corresponded to six bright fringes and six dark fringes that passed over the pixel. The values of $I(t)_{(200,400)}$ stabilized from approximately 0.25 h and gradually decreased while fluctuating. These results were coincident with those from the spatio-temporal image in **Fig. 3 (c)**.

In the 2nd step, the maximum intensity $I_{\max(200,400)}$ and minimum intensity $I_{\min(200,400)}$ were detected as shown in **Fig. 5 (a)**. The value of $I_{\min(200,400)}$ was obtained at approximately 0.1 h during large changes in intensity. On the other hand, the value of $I_{\max(200,400)}$ was obtained at approximately 0.5 h during fluctuating intensity and it was one of the specific intensity changes.

In the 3rd step, the values of $I(t)_{(200,400)}$ could be converted

into phase $\phi(t)_{(200,400)}$ as shown in **Fig. 5 (b)** based on Eq. 3. The values of $\phi(t)_{(200,400)}$ changed largely from approximately 0.03 h to 0.15 h and they fluctuated from approximately 0.25 h. These results were coincident with the result in the first step. However, the almost peak values of $\phi(t)_{(200,400)}$ from approximately t = 0.03 h to 0.15 h were not the ideal ones, that is, neither −π/2 nor π/2. There are two main reasons for these differences. The first is the intervals of alternative irradiation by the two laser beams. The centers of the bright and dark fringes may have passed over the pixel (200, 400) within 3 s of the intervals. The second is the specific changes in intensity, such as the one at approximately 0.5 h in **Fig. 5 (a)**. When such a specific large (or small) intensity is detected as $I_{\max_{(X,Y)}}$ (or $I_{\min_{(X,Y)}}$) in the second step, the values of $\phi(t)_{(X,Y)}$ are relatively small (or large) in the third step. Hence, the peak values differed from the ideal values. The specific intensity was caused by the disturbance of the air flow around the sample module.

In the 4th step, the peak values $\phi_{\mathrm{P}_{(200,400)}}$ of the phase from approximately 0.02 h to 0.16 h were automatically detected by using *findpeaks* function in MATLAB® as shown in **Fig. 5 (b)**. The values $\phi_{\mathrm{P_k}}$ correspond to the k-th detected peak values. Blank red circles correspond to the correct peak values, which agreed with the results from the spatio-temporal image. On the other hand, blank blue squares correspond to the fake peak values, which disagreed with the results from the spatio-temporal image and should not be considered as peak values. As a result, the total number of detected peak values was thirty-seven, that is, n = 37, which was approximately three times larger than that from the spatio-temporal image, that is, n = 12.

In the 5th step, the values of $\phi(t)_{(200,400)}$ were unwrapped thirty-seven times. The values of $\phi'(t)_{(200,400)}$ were obtained as shown in **Fig. 5 (c)**. The thin dotted line shows the original phase as shown in **Fig. 5 (b)**. The solid line shows the result after unwrapping thirty-seven times. The proposed unwrapping algorithm enabled us to unwrap the values of $\phi(t)_{(200,400)}$ for n times symmetrically.

In the 6th step, as a result, the value of $\Delta\phi_{(200,400)}$ was obtained as $36.9\,\pi$ rad by subtracting the value of $\phi'(0\text{ h})_{(200,400)}$ from the value of $\phi'(7\text{ h})_{(200,400)}$ (**Fig. 5 (d)**) while the reference one obtained by the thinning method was $12.3\,\pi$ rad. The value of $\Delta\phi_{(200,400)}$ obtained by the proposed method was three times larger than that obtained by the thinning method, and the result was coincident with that of the number of detected peak values mentioned above. Therefore, the large value of $\Delta\phi_{(200,400)}$ was caused by detecting fake peak values as real peak ones in the 4th step.

The phase change in a line Y = 400 $\Delta\phi_{(X,400)}$ could be obtained as shown in **Fig. 6**. The horizontal axis corresponds to the pixels in the vertical axis X of the image. The black squares and red circles correspond to the results obtained by the proposed method in this study and the thinning method, respectively. As a result, all results obtained by the proposed method in this study were fluttered towards the upper side against the reference ones.

The calculation time from the 1st step to the 5th step in a line Y = 400 was approximately 10 s. On the other hand, the thinning method took approximately 2 h to obtain four values of $\Delta\phi_{(X,Y)}$. Therefore, by using the method proposed in this study, the proceeding speed for obtaining values of $\Delta\phi_{(X,Y)}$ could be dramatically improved. However, the discrepancy of the values of $\Delta\phi_{(X,Y)}$ obtained by the proposed method and those by the thinning method is discussed in the following section.

4. Discussion for Exclusion of High-Frequency Temporal Noise

In **Fig. 6**, all the values of $\Delta\phi_{(X,Y)}$ obtained by the proposed method in this study were larger than the reference ones. It was caused by detecting fake peak values as real peak ones in the 4th step. Fake peak values led to excessive fake unwrapping in the 5th step and the values of $\Delta\phi_{(X,Y)}$ were larger than the references. Therefore, excluding fake peak values is necessary for obtaining accurate values of $\Delta\phi_{(X,Y)}$. To exclude fake peak values, two kinds of filters and a threshold for peak values were considered. A spatial filter and a temporal filter were applied to interference fringe images and the phase $\phi(t)_{(X,Y)}$ for smoothing their distributions. In the process, *gaussfilt* and *conv2* functions in MATLAB® were used for the spatial filter and the temporal filter, respectively. The standard deviations of the spatial and temporal filters were defined as σ_s and σ_t, respectively. The values of σ_s and σ_t correspond to the degree of smoothing. **Figure 7** shows the relationship between the spatial distribution of intensity in a line Y = 400 and the standard deviation σ_s of the spatial filter. **Figures 7 (a) to (d)** correspond to the results of $\sigma_s = 2$ to 5, respectively. In **Figs. 7 (c) and (d)**, the splits of peak values at approximately X = 100 and 300 in

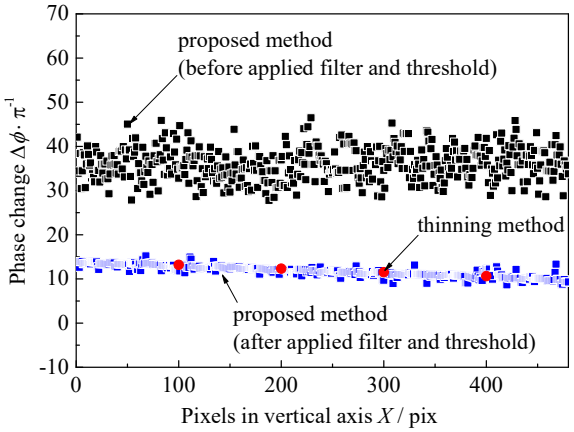

Fig. 6 Phase change $\Delta\phi_{(X,Y)}$ normalized by π rad in a line Y = 400 in wavelength 532 nm. Black and blue squares plot the results obtained by the proposed method before and after processed through filters and a threshold, respectively. Circles plot the results obtained by the thinning method.

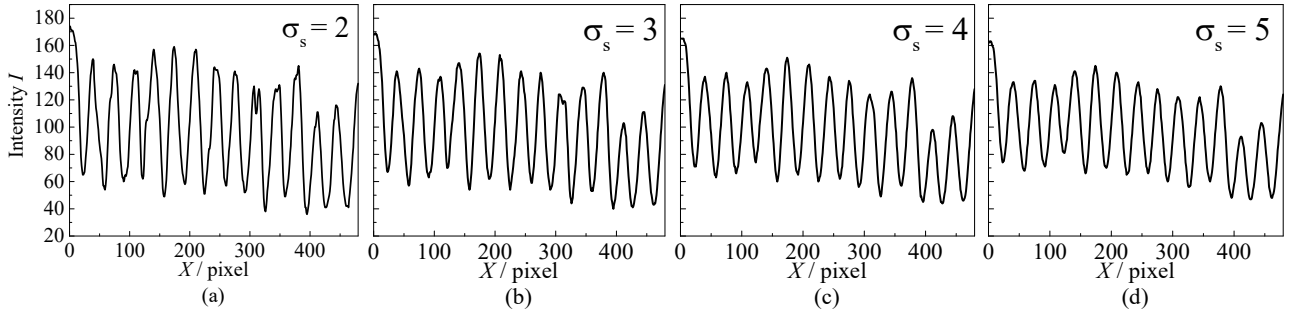

Fig. 7 Spatial distribution of intensity in a line $Y = 400$ in wavelength 532 nm with the various standard deviations of the spatial filter (a) $\sigma_s = 2$, (b) $\sigma_s = 3$, (c) $\sigma_s = 4$, and (d) $\sigma_s = 5$.

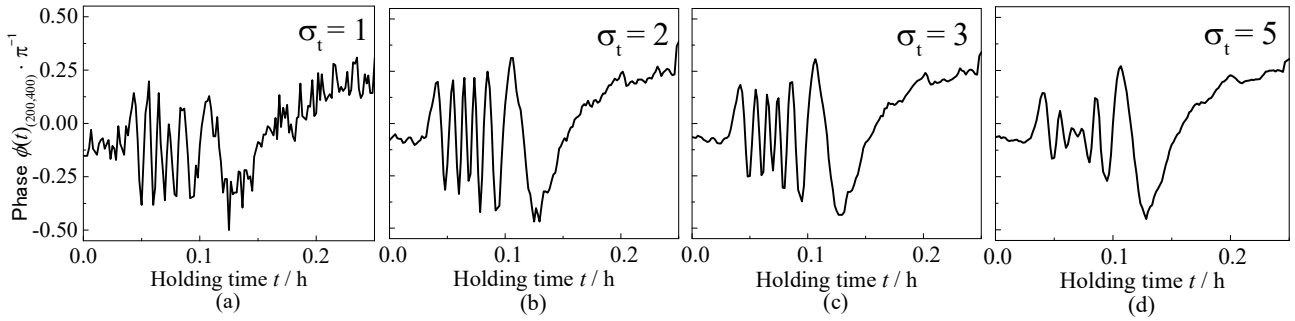

Fig. 8 Relationship between the distribution of phase $\phi(t)_{(200,400)}$ normalized by π rad of wavelength 532 nm and the holding time with the various standard deviations of the temporal filter (a) $\sigma_t = 1$, (b) $\sigma_t = 2$, (c) $\sigma_t = 3$, and (d) $\sigma_t = 5$.

Fig. 7 (a) were combined, and the degree of smoothing became large compared with **Figs. 7 (a) and (b)**. **Figure 8** shows the relationship between the distribution of phase $\phi_{(X,Y)}$ and the standard deviation σ_t of the temporal filter. **Figures 8 (a) to (d)** correspond to the results of $\sigma_s = 1$, 2,3, and 5, respectively. In **Figs. 8 (c) and (d)**, the degree of smoothing became large compared with **Fig. 8 (a)**. However, in **Fig. 8 (d)**, the strength of peak values from approximately 0.05 h to 0.1 h became small compared with **Figs. 8 (b) and (c)**. Therefore, choosing suitable combinations of the values of σ_s and σ_t is critical to exclude fake peak values.

In addition, to exclude fake peak values even after processing through these filters, the threshold for peak values was considered. **Figure 9** explains the definition of the threshold. In the setting process of the threshold, the *k*–th detected peak values $\phi(t'_k)_{(X,Y)}$ were focused on. The differences between the peak values and the values of $\phi(t'_k - 6E_{ra})_{(X,Y)}$, which were E_{ra} capturing intervals away from the focused peak values, were obtained. The value of $t'(= t \cdot 3600\ \mathrm{s})$ corresponds to the holding time and a capturing interval is 6 s in this study (**Fig. 3 (b)**). The focused *k*-th peak values were fake ones when the differences were smaller than the values of threshold, that is, $\left|\phi(t'_k)_{(X,Y)} - \phi(t'_k - 6E_{ra})_{(X,Y)}\right| < E_{th}$, and the peak values were excluded. The combinations of the values of E_{th} and E_{ra} correspond to the degree of sharpness of the peak values: larger E_{th} and smaller E_{ra} correspond to sharper peak values.

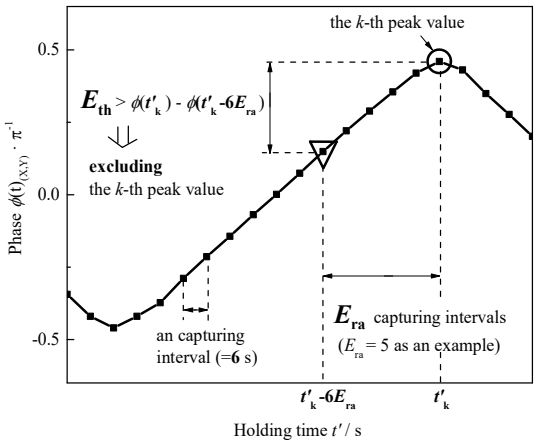

Fig. 9 Schematic of the simulated phase to explain the parameters of processing through a threshold. A circle plots the *k*–th detected peak value $\phi(t'_k)_{(X,Y)}$, and reverse triangles plot the values of $\phi(t'_k - 6E_{ra})_{(X,Y)}$ which are E_{ra} capturing intervals away from the focused peak value and the value of $t'(= t \cdot 3600\ \mathrm{s})$ corresponds to the holding time. The value of E_{th} is a threshold for the difference of these phases $\phi(t'_k)_{(X,Y)} - \phi(t'_k - 6E_{ra})_{(X,Y)}$ ($\phi(t'_k)_{(X,Y)} - \phi(t'_k - 6E_{ra})_{(X,Y)} < E_{th}$ means that the focused peak value is a fake one).

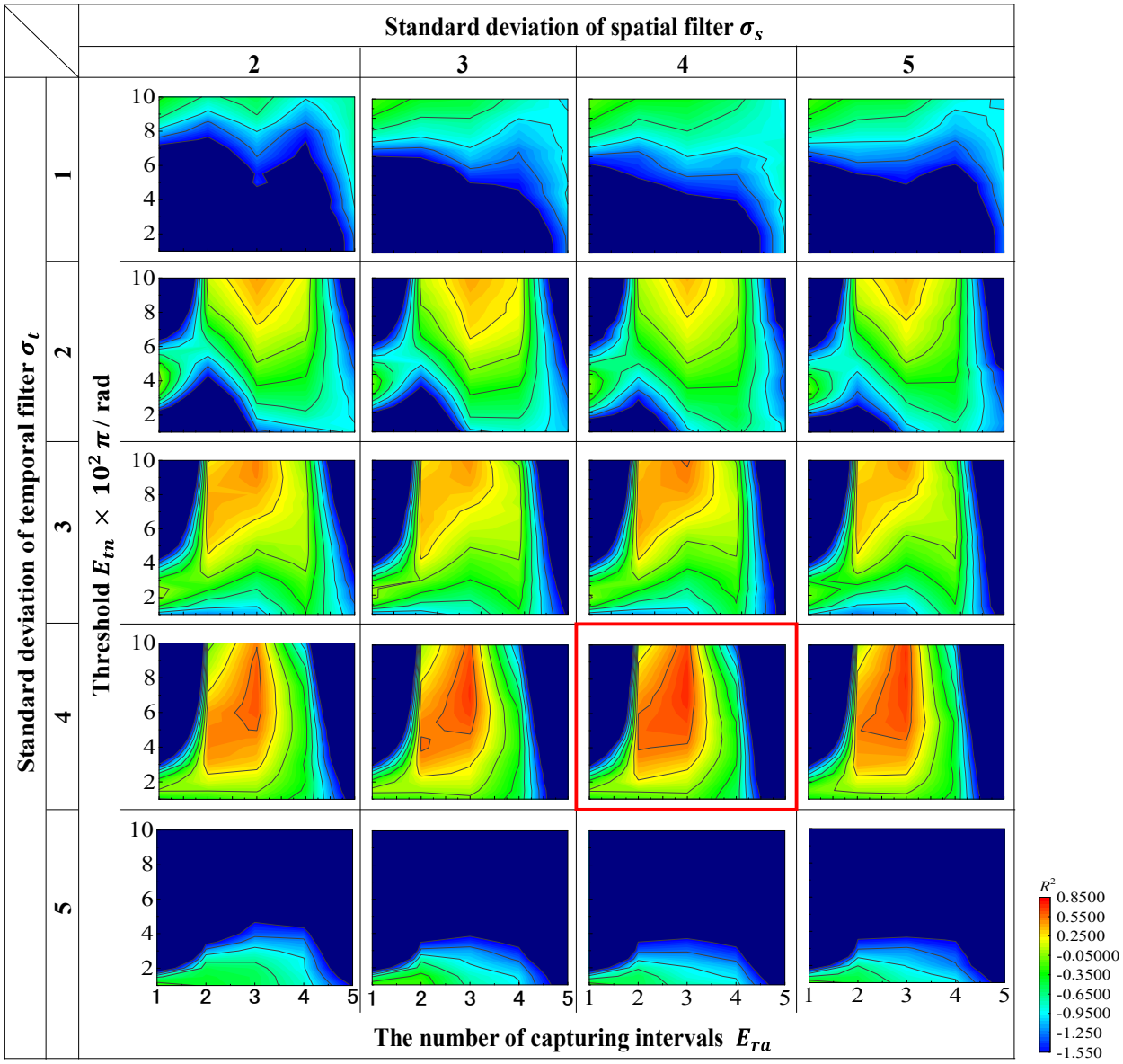

Fig. 10 Coefficients of determination R^2 of the various combinations of $(\sigma_s, \sigma_t, E_{th}, E_{ra})$. The values of R^2 show the degree of coincidence between the gradient of the phase change $\nabla(\Delta\phi_{(X,400)})$ obtained by the proposed method and that obtained by the thinning method in a line $Y = 400$ in the wavelength 532 nm. The values σ_s and σ_t correspond to the standard deviations of spatial and temporal filters, respectively. The values of E_{th} and E_{ra} correspond to the values of the threshold and the number of the capturing intervals, respectively. Red square block shows the most suitable combination for exclusion of fake peak values of wavelength 532 nm.

These filters and the threshold with 1000 combinations of $(\sigma_s, \sigma_t, E_{th}, E_{ra})$ were then applied to a spatio-temporal image in a line $Y = 400$: σ_s = 2 to 5 (four conditions), σ_t = 1 to 5 (five conditions), $E_{th} \cdot \pi$ = 0.01 to 0.1 (ten conditions), and E_{ra} = 1 to 5 (five conditions). **Figure 10** shows the relationship between the coefficient of determination R^2 and the combinations of $(\sigma_s, \sigma_t, E_{th}, E_{ra})$. The value of R^2 is a parameter, which is calculated by subtracting the residual sum of squares from 1, and therefore increases with decreasing residual error of fitting. The values of R^2 close to 1 corresponds to a good fit. The calculated values of R^2 shows the degree of coincidence between the gradient of phase change $\nabla(\Delta\phi_{(X,400)})$ obtained by the proposed method and that obtained by the thinning method. In **Fig. 10**, the tendency and the values of R^2 did not change according to the values of σ_s in the same values of σ_t. This result indicated that the degree of the spatial filter did not have a clear effect on excluding fake peak values. On the other hand, focusing on the values of σ_t, the values of R^2 are obviously

large at $\sigma_t = 4$. This was because the degrees of smoothing were not enough under the conditions with $\sigma_t < 4$ and the degree of smoothing was too large to retain the strength of peak values under the conditions with $\sigma_t > 4$. In **Fig. 10**, a high R^2 value can be obtained with the following combination in a line Y = 400 in wavelength 532 nm: $(\sigma_s, \sigma_t, E_{th}, E_{ra}) = (4, 4, 0.08 \cdot \pi^{-1}, 3)$. **Figure 11** shows the result of detected peak values (4th step) of the phase $\phi(t)_{(200,400)}$ after processing through the filters and the threshold with $(\sigma_s, \sigma_t, E_{th}, E_{ra}) = (4, 4, 0.08 \cdot \pi^{-1}, 3)$. The fake peak values detected in **Fig. 5 (b)** could be excluded and twelve correct peak values could be accurately detected. In **Fig. 6**, blue squares plot the values of $\Delta\phi_{(X,400)}$ after processing through the filters and the threshold. The values of $\Delta\phi_{(X,400)}$ became obviously suitable compared to results before processing through the filters and the threshold (black squares). Therefore, applying these filters and the threshold were confirmed to be effective for obtaining accurate values of $\Delta\phi_{(X,Y)}$. This most suitable combination of the parameters $(\sigma_s, \sigma_t, E_{th}, E_{ra})$ for these filters and the threshold could be obtained automatically in MATLAB®. For the consideration of the universality of the suitable combination, these filters and the threshold with deferent combinations of $(\sigma_s, \sigma_t, E_{th}, E_{ra})$ were applied to a spatio-temporal image in a line Y = 400 in wavelength 780 nm. The values of $(\sigma_s, \sigma_t, E_{th}, E_{ra}) = (5, 2, 0.08 \cdot \pi^{-1}, 6)$ could be obtained as the most suitable combination. As a result, the most suitable combinations could be obtained automatically at different wavelengths. However, these suitable parameters were confirmed not to be universal. These additional processes were shown as green blocks with a double square in **Fig. 4**.

The values of $\Delta\phi_{(X,Y)}$ in pixels of the whole observation area in wavelengths 532 nm and 780 nm could be obtained by applying the filters and the threshold with each suitable combination of the parameters as shown in **Figs. 12 (a) and (b)**, respectively. **Figures 12 (a) and (b)** show the results processed through additional filters to smooth the noise. The pixels at $Y <$ 70 correspond to the glass walls and those at $Y >$ 70 correspond to the sample solution through glass walls.

Even after applying the filters and a threshold, the calculation time from the 1st step to the 5th step in a line Y = 400 was approximately 10 s, and that in pixels of the whole observation area was approximately 600 s. Furthermore, the detecting time of the suitable parameters for the filters and a threshold was approximately 900 s for 1000 conditions in this study. These calculations were conducted by using a software MATLAB® with a PC (Windows 7 Professional®, Intel® Xeon® CPU E5-1650 v2 @ 3.50 GHz, 64.0 GB). The total processing time

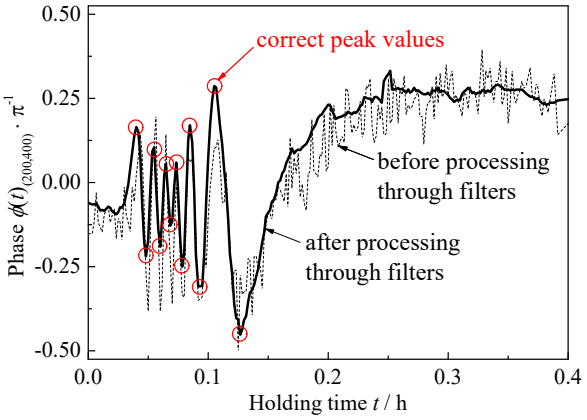

Fig. 11 Phase change $\Delta\phi$ in a line Y = 400 in wavelength 532 nm. Dotted and bold lines show the original before and after processing through filters ($\sigma_s = 4$ and $\sigma_t = 4$), respectively. Red circles plot the detected correct peak values after processing through a threshold ($E_{th} = 0.08 \cdot \pi^{-1}$ and $E_{ra} = 3$).

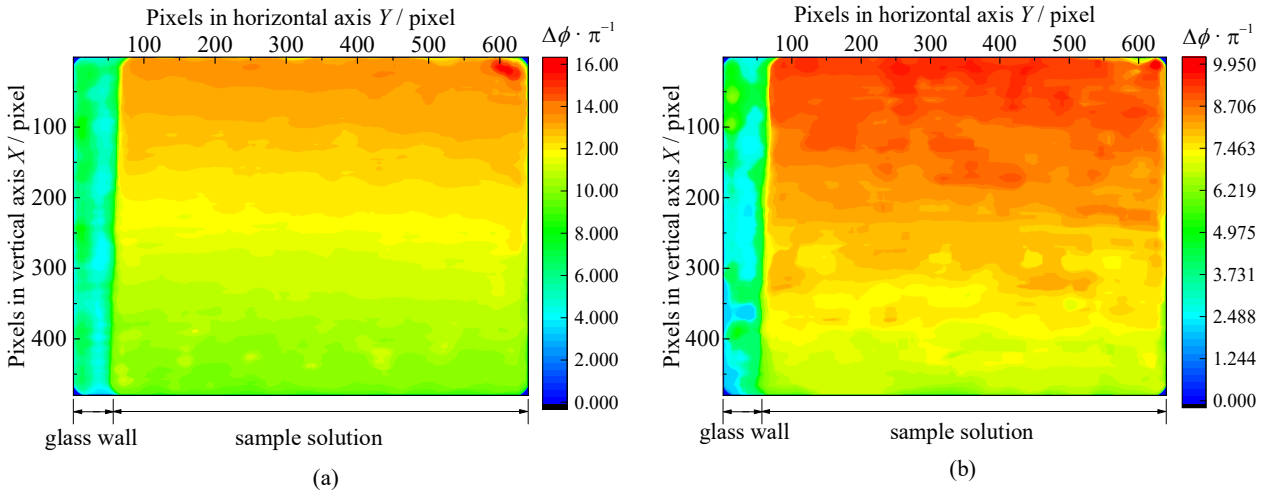

Fig. 12 Color mappings of the phase change $\Delta\phi_{(X,Y)}$ in a whole observation area of wavelengths 532 nm (a) and 780 nm (b) after processing through the filters and the threshold and an additional filter for smoothing spatial noises.

including detection of suitable parameters and calculation of the values of $\Delta\phi_{(X,Y)}$ in pixels of the whole observation area was approximately 1500 s. This processing time was one-fifth of the calculation time for obtaining four values of $\Delta\phi_{(X,Y)}$ by the thinning method.

Therefore, the method proposed in this study could dramatically improve processing speed and enlarge analyzing areas for obtaining the phase change $\Delta\phi_{(X,Y)}$.

5. Conclusion

This paper confirmed the effectiveness of the proposed method as the following:

1) The simple phase analysis method using spatio-temporal images of interference fringes developed in this study enabled us to obtain the values of $\Delta\phi_{(X,Y)}$ in the whole observation area automatically approximately 600 s in MATLAB®. It could dramatically improve the processing speed and enlarge analyzing areas compared to the thinning method.
2) For the accurate unwrapping of phase, smoothing distribution of the fringes by spatial and temporal filters and excluding the fake peak values through a threshold were confirmed to be necessary. The most suitable combinations of parameters for these filters and the threshold could be determined automatically in approximately 900 s.
3) The proposed method could be applied to the analysis of different fringe conditions by determining the most suitable combinations of the parameters automatically in each analysis.

Acknowledgments

This study was supported by Japan Aerospace Exploration Agency Working group on “Diffusion Phenomena in Melts.” We would like to gratefully thank Dr. S. Adachi (JAXA) and Dr. T. Shimaoka (JSF) for helpful discussions, and the members of JEM Utilization Center, JAXA Flight Control Team (JFCT) and FISICS, and the crew members of ISS Expedition 40 for operation of the experiments.

References

1) Y. Inatomi: J. Jpn. Soc. Microgravity Appl. **28** (2011) 155.
2) M. Tomaru, T. Osada, I. Orikasa, S. Suzuki and Y. Inatomi: Microgravity Sci. Technol., **31** (2019) 49.
3) Y. Inatomi, I. Yoshizaki, K. Sakata, T. Shimaoka, T. Sone, T. Tomobe, S. Adachi, S. Yoda and Y. Yoshimura: Defect Diffus. Forum, **323** (2012) 533.
4) Y. Inatomi, M. Ashida, K. Sakata, J. Wang and T. Okutani: J. Jap. Assoc. Crystal Growth, **39** (2012) 11 (in Japanese).
5) T. Osada, Y. Hashimoto, M. Tomaru, S. Suzuki, Y. Inatomi, Y. Ito and T. Shimaoka: Int. J. Microgravity Sci. Appl., **33** (2016) 330407.
6) Y. Mori, Y. Hashimoto, S. Suzuki, Y. Inatomi, Y. Ito and T. Shimaoka: Trans. Jpn. Soc. Aeron. Space Sci., **12** (2014) 37.
7) Y. Morimoto, T. Matsui and M. Fujigaki: Comp. Vis. Ima. Med., **47** (2006) 10.
8) P. Hariharan, B. F. Oreb and T. Eiju: Appl. Opt., **26** 13 (1987) 2504.
9) K. Tsukamoto: Oyo Buturi, **63** (1994) 713 (in Japanese).
10) M. Takeda, H. Ina and S. Kobayashi: J. Opt. Soc. Am., **72** 1 (1982) 156.
11) A. Mialdun and V. Shevtsova: Int. J. Heat Mass Transf., **51** (2008) 3164.
12) A. Mialdun and V. Shevtsova: J. Chem. Phys. **134** (2011) 044524.
13) A. Mialdun, C. Minetti, Y. Gaponenko, V. Shevtsova and F. Dubois: Microgravity Sci. Technol., **25** (2013) 83.
14) K. Creath: Progress in Optics, edited by E. Wolf (North-Holland, Amsterdam), **26** (1988) 349.